Research Progress of Tip/Tilts Control Bandwidth Promotion for Beam Combining Application in IOE, CAS

Guan Huang[1,2,3], Feng Li[1,2], Chao Geng[1,2], Xinyang Li[1,2] and Jiaying Liu[1,2,3]
[1]*Institute of Optics and Electronics, Chinese Academy of Sciences, Chengdu, Sichuan 610209, China*
[2]*Key Laboratory on Adaptive Optics, Chinese Academy of Sciences, Chengdu, Sichuan 610209, China*
[3]*University of Chinese Academy of Sciences, Beijing 100049, China*

Keywords: Beam Combining, Tip/Tilts Control, Adaptive Fiber Coupling, Fiber Optics.

Abstract: Fiber-array beam director composed of numerous fiber collimators gives out excellent adaptive optics (AO) performance better than traditional AO-enhanced monolithic director owe to the extremely high bandwidth of the fiber-integrated phase modulator. For fiber laser transmission applications represented by coherent-beam-combining, correction of sub-aperture tip/tilts is needed to further promote the combined beam's quality besides the phase-locking control. For power reception of the incident laser beam, tip/tilts control is indispensable to ensure efficient and stable laser beam coupled from space into fiber. Here, we adopt adaptive fiber optics collimator as the tip/tilts device, which owns advantages of precise control, small inertia and convenience for packaging. While most existed tip/tilts control methods are restricted to optimization algorithms which suffer from disadvantages of low bandwidth utilization ratio. In this paper, research progress of tip/tilts control bandwidth promotion for beam combining applications in IOE, CAS is presented. Methods of inherent response delay compensation and active resonance suppression are proposed and experimentally validated. The experimental results give great prospects to future applications that utilize fiber-collimators-array as optical transceivers.

1 INTRODUCTION

In recent years, novel fiber-array beam director (BD) with an array of densely packed and conformal fiber collimators has caused great interests and deep researches (Filimonov et al., 2014). Such fiber-array beam director could transmit coherent multi-laser-beams from the same seed laser to form diffraction spot with size equivalent to what we can get through conventional BD with the same aperture diameter (Vorontsov et al., 2009). This technique is a common approach in directed energy application based on fiber laser coherent-beam-combining (CBC), which is aimed at promoting the laser output power which is limited by various nonlinear effects in fiber, like SBS and thermally-induced-mode-instability (Yu et al., 2013). Fiber-array BD also has prospects in other laser beam projection systems, such as remote power beaming, free space laser communications and active imaging. One of the main controversial issues about fiber-array BD is that the unavoidable power distributed in the side-lobes takes up a significant part of the total source power. Problem of strong side-lobe effect is caused by the sparse nature of the fiber-array BD of truncated Gaussian beams. According to recent numerical simulations and experimental researches (Vorontsov et al., 2016), the fiber-array BD gives out better performance under atmospheric turbulence when compared with traditional adaptive-optics-enhanced Cassegrain-type telescope with the same aperture area. The adaptive optics (AO) ability of the fiber-array BD is integrated in the sub-apertures where the sub-aperture-averaged phase distortions named as pistons could be compensated, also named phase-locked, through fiber-integrated phase modulator with ultra-high bandwidth approaching GHz (Weyrauch et al., 2016). Phase-distortions here are mainly caused by the inner fiber laser amplifiers, environmental vibrations, and the external dynamic turbulence. Meanwhile, tip/tilt errors correction attracts increasing interests because people find that the coherent combined laser beam's quality of the fiber-array BD needs further promotion beyond the phase-locking control (Geng et al., 2013). In fact, pointing error caused by the machining error and

Huang, G., Li, F., Geng, C., Li, X. and Liu, J.
Research Progress of Tip/Tilts Control Bandwidth Promotion for Beam Combining Application in IOE, CAS.
DOI: 10.5220/0007377100520058
In *Proceedings of the 7th International Conference on Photonics, Optics and Laser Technology (PHOTOPTICS 2019)*, pages 52-58
ISBN: 978-989-758-364-3

assembly error is unavoidable considering the numerous collimators and constricted sub-aperture space. Meanwhile, platform vibration and turbulence-induced dynamic sub-aperture tip/tilt errors further degrade the quality of the combined beams (Geng et al., 2013).

Another strong argument against the fiber-array BD technique is that it's hard to be utilized as a beam receiver. Incidence laser beam is divided into each sub-aperture and then forms numerous sub-beams which are isolated to each other in space. Spatial resolution here is extremely degraded and confined to the diffraction-limited resolution of the single sub-aperture. This is different from traditional telescope where angular resolution of the outgoing beam and the incident beam are the same, because they share the same aperture with the help of beam splitter. This gives challenges to the fiber-array BD to precisely track the target. Precise tracking needs resolution of λ/D (λ is the working wavelength, D is the diameter of the array's synthetic aperture), while only resolution of λ/d could be achieved in fact. But recent progress on techniques of multi-aperture laser transceiving reported by IOE, CAS gives out new ideas on such issues (Li et al., 2017). In such methods, laser beam coupling from space into fiber is achieved in all the sub-apertures in the fiber-array BD (Luo et al., 2014). The total power of the incident laser beam of the whole aperture then could be obtained by collecting all of the coupled laser beam in sub-apertures (Yang et al., 2017). This application shows great prospects in free-space-laser communication systems (Yang et al., 2017). The coupling efficiency here is highly influenced by the tip/tilts in the sub-aperture, which make the displacement between the focal spot and the fiber core (Li et al., 2015). Fast and efficient tip/tilts correction is indispensable especially when facing atmospheric turbulence, because tip/tilt-type errors take up the most part (almost 87%) of the aberrations for Kolmogorov turbulence.

Owning to the unique characters of compact and sparse apertures, there are few options to execute the tip/tilts control. Novel fiber device named adaptive fiber-optics collimator (AFOC) is one of the most promising tip/tilts devices (Liu et al., 2007). This device contains a collimating lens, a cross-beam and four bimorph piezoelectric actuators. The tip of the fiber is fixed in the central hole of the cross beam, deviated in the rear focal plane of the collimating lens. This structure has advantages of precise control, small inertia and ability for array extension. More important, it's suitable for both the outgoing and incident laser beam (Geng et al., 2011). Different from the high-bandwidth fiber-integrated phase modulator, AFOC suffers from low bandwidth. Control of the pistons of the fiber-array BD relies on blind optimization algorithms like stochastic parallel gradient descent (SPGD) algorithm, which works with low bandwidth utilization ratio. There are two main reasons for the limited iteration rate in the tip/tilts control loop. Firstly, as a typical bimorph-based device, the operational frequency bandwidth of AFOC is restricted with resonances, where the amplitude of the induced deviation can increase significantly up to a level where the device will be broken (Beresnev et al., 2005). Secondly, researches by IOE CAS show that there exists an inherent response delay in the tip/tilts control loop, which could lead to the fuzzy gradient estimation result during the high-speed iteration process of SPGD (Huang et al., 2018).

Methods which could be more efficient in utilizing the limited bandwidth of the AFOC are in urgent need. In fact, tip/tilts control for the outgoing and incident laser beam are concurrent according to the optical reversibility principle. When the best coupling is obtained, precise pointing to the target could be achieved simultaneously. At the same time, such processes in each sub-aperture are independent from each other. Then bandwidth utilization ratio of the AFOC could be promoted. In this paper, the research progress of tip/tilts control promotion for both the laser beam coupling and CBC in the fiber-array BD in IOE, CAS is presented.

2 INHERENT RESPONSE DELAY COMPENSATION

Here, we present the recent work of promoting the effective bandwidth of tip/tilts control using AFOC for adaptive fiber coupling. Such improved method is named precise-delayed SPGD (PD-SPGD). Experimental demonstrations are executed in atmosphere cooperating with traditional AO system.

Figure 1 shows the structural scheme of adaptive coupling system based on AFOC. The laser beam with plane wavefront is focused and coupled into a controlled tip of single-mode-fiber (SMF) by AFOC, part of the coupled optical power is sent to the communication receiver and another is converted to voltage by a photodetector. This voltage is transferred to the controller and used as performance metrics. Two channels of control voltages from the controller are amplified one hundred times by the

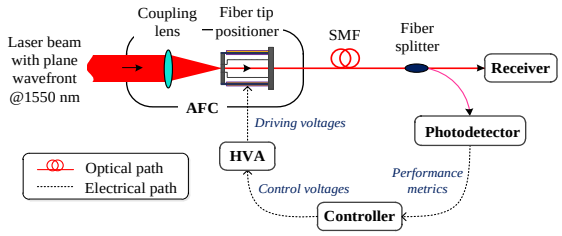

Figure 1: Structural scheme of adaptive coupling system based on AFOC.

high-voltage amplifier (HVA) and then drive the AFOC to realize closed loop control.

In the control loop of AFOC system, the inherent response delay we tested is about 96 μs. Consequently, a threshold of the iteration rate is about 5 kHz. To solve this problem, PD-SPGD is proposed. In this algorithm, the sampling rate of the performance metrics is set to many times (hereafter refer to as *K*) of the iteration rate, and these metrics captured during the several historical iterations (hereafter refer to as *M*) are recorded in the controller memory. Therefore, we can get a sequence of performance metrics at each iteration (*n*), represented here as $J_0^{(n)}$, $J_1^{(n)}$,…, $J_{MK}^{(n)}$. Then, we can take a specific selection from these metrics to perform the gradient estimation, and update the control voltages from $\mathbf{U}^{(n)}$ to $\mathbf{U}^{(n+1)}$, as shown in following Eq. (1) and Eq. (2):

$$\mathbf{U}^{(n+1)} = \mathbf{U}^{(n)} + \gamma \Delta \mathbf{U}^{(n-\Delta n)} \left[J_p^{(n)} - J_{p+K/2}^{(n)} \right] \quad (1)$$

$$\Delta n = \text{int} \left\langle \frac{\tau_{resp} + \tau_{spgd} / 4}{\tau_{spgd}} \right\rangle \ , \ p = \text{int} \left\langle K \frac{\tau_{resp} + \tau_{spgd} / 4}{\tau_{spgd}} \right\rangle \quad (2)$$

Here, τ_{resp} and τ_{spgd} are the iteration interval of SPGD algorithm and the inherent response delay, respectively. $\Delta\mathbf{U}^{(n-\Delta n)}$ is the random perturbations disturbed in the iteration (n-Δn). $J_p^{(n)}$ and $J_{p+K/2}^{(n)}$ are the selected metrics that corresponding to the disturbed voltages $\mathbf{U}^{(n-\Delta n)} + \Delta\mathbf{U}^{(n-\Delta n)}$ and $\mathbf{U}^{(n-\Delta n)} - \Delta\mathbf{U}^{(n-\Delta n)}$. The newly added two parameters Δn and p are defined as the integral-delay parameter and the precise-delay parameter respectively. The operator "int < >" used in Eq. (2) denotes integer conversion. In addition, to ensure that all these metrics are sampled during the period between the disturbed voltages change and the corresponding metrics response, parameter *M* is usually set to Δn+1. Parameter *K* is usually set to an integer bigger than 10, to provide enough compensation accuracy of PD-SPGD algorithm.

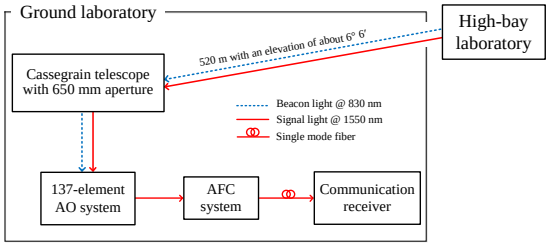

Figure 2: Schematic of the experimental setup and the optical path used in the actual atmospheric compensation experiments.

The AFOC coupling control system cooperates with traditional AO system in free space laser communication system has been demonstrated. The experimental setup of the system is shown in Figure 2. These two systems and the telescope were located at a ground laboratory on one side, the beacon light and signal light emission equipment was located at the high-bay laboratory building on the other side. Beacon light with a wavelength of 830 nm was used for AO and signal light with a wavelength of 1550 nm was used for beam coupling and communication. These two kinds of light were received by a Cassegrain telescope. The AO system contains a 137-element deformable mirror, a FSM, a Hartmann-Shack wavefront sensor, and a wavefront controller. The AO system here has a 0 dB error suppression bandwidth of about 50 Hz. The structural parameters of the AFOC system were the same as above and the PD-SPGD algorithm with iteration rate of 8 kHz was used.

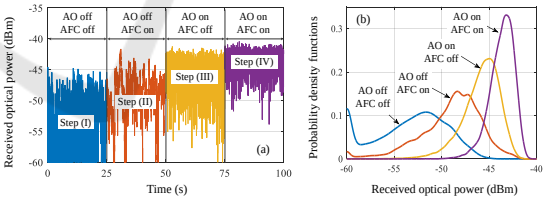

Figure 3: (a) Sample evolution curve of received optical power in dependence on the time. (b) Probability density functions (PDFs) calculated from measured optical power values for the four different operation conditions.

Figure 3 shows experimental results performed under relatively strong turbulence conditions (Fried parameter r_0 is 2.6 cm). The operation status of the two systems contains four different steps: (I) two systems didn't perform any correction; (II) only the AFOC correction was performed; (III) only AO correction was performed; (IV) both AFOC and AO performed corrections. Figure 3(a) shows a sample evolution curve for the received optical power, which is measured at the receiver port of AFOC

system. By means of only correcting static angular errors and angular jitters with AFOC system in step (II), the average of optical power is increased from -51.53 dBm to -47.57 dBm; when the higher-order aberrations is corrected by AO system in step (III), this value becomes -44.98 dBm; finally, when two systems work simultaneously in step (IV), the average of received optical power reaches the optimal value, that is -43.00 dBm. It can be calculated that compared to the previous step, the average value of optical power went up by 3.95 dB in step (II) and went up by 1.98 dB in step (IV). The dithering range of optical power in step (I) is 15.86 dB; this index is slightly worse in step (II) and step (III), which are 18.81 dB and 19.21 dB; the dithering range is suppressed to the optimal value when both systems are closed in step (IV), which is 13.44 dB. Figure 3(b) presents the probability density functions (PDFs) of the received optical power, calculated for each of the four different operation conditions. The PDF in step (I) is wide and bumpy, which indicates that the coupling efficiency is unstable and degraded by the atmospheric turbulence; these curves gradually become narrower and shift to larger optical power direction in subsequent steps, which indicates that the stable and promoted coupling efficiency is achieved. Figure 4 shows the eye patterns during the four control processes correspond to that shown in Figure 3(a).

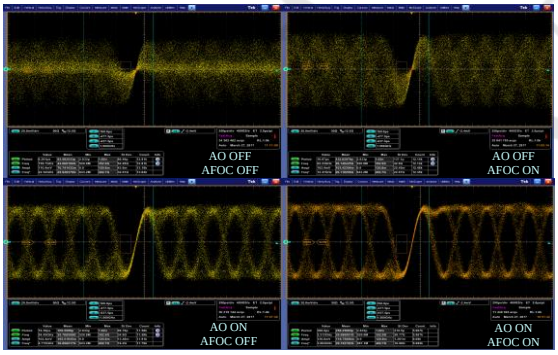

Figure 4: Eye patterns during the four control processes correspond to that shown in Figure 3(a).

The above experimental results show that the AFOC system can effectively improve the average value of received optical power and suppress the power fluctuation in both cases of AO system off and on. The advantage of this control structure is that it could correct the misalignment errors caused by the movement of the receiving platform, and it also has a stronger inhibitory effect on the dithering of focused spot which comes from the tip/tilt residual errors of AO system.

3 ACTIVE RESONANCE SUPPRESSION

Experiment in part 2 is focused on solving the inherent time delay in the AFOC control and increasing the bandwidth under which the SPGD algorithm could work. But time delay is not the only problem that is needed to be solved. Resonance effect is inevitable and decides that the SPGD could only work under frequency lower than the first order resonance frequency. Here we present the research progress of compensating the resonance effect to obtain better performance in IOE, CAS.

Existed researches show that the transfer function model of AFOC can be represented by the combination model $F_{CM}(s)$ with four biquad oscillation elements and an inherent response delay element $e^{-(8.8e-05)s}$. Therefore, for each biquad oscillation element $F_k(s)$, if there exists a biquad filter $F_{BFk}(s)$ with the exact opposite frequency characteristics of $F_k(s)$, then the resonance composition caused by this oscillation element can be compensated by cascading $F_{BFk}(s)$. The detailed form of $F_{BFk}(s)$ is shown in Eq. (3):

$$F_{BFk}(s)=\frac{1}{F_k(s)}=\left[\frac{s^2/\omega_{pk}^2+2\xi_{pk}s/\omega_{pk}+1}{s^2/\omega_{zk}^2+2\xi_{zk}s/\omega_{zk}+1}\right] \quad (3)$$

Furthermore, if there exists such four biquad filters $F_{BFk}(s)$ with the exact opposite frequency characteristics of each $F_k(s)$, then the transfer function of AFOC can be compensated to a pure delay system. Here, $F_{BF}^m(s)$ is used to represent the combination of the former m biquad filters, as shown in Eq. (4). The frequency characteristics of $F_{BF}^m(s)$ and the compensated system $F_{AFOC}(s)\cdot F_{BF}^m(s)$ obtained through simulations are shown in Figure 5.

$$F_{BF}^m(s)=\prod_{k=1}^{m}F_{BFk}(s) \quad (4)$$

Figure 5(a) shows the amplitude-frequency characteristic of the combination of the former m biquad filters, and Figure 5(b) shows the amplitude-frequency characteristic of the AFOC after being compensated by such filters. Figure 5(b) indicates that as the parameter m (the number of filters used) increases, the resonance peak of the compensated system gradually flattens out and moves toward the high frequency direction. Figure 5(c) and Figure 5(d) shows the corresponding phase-frequency characteristic. In Figure 5(d), the curve tends to be linear as m increases. It indicates that the

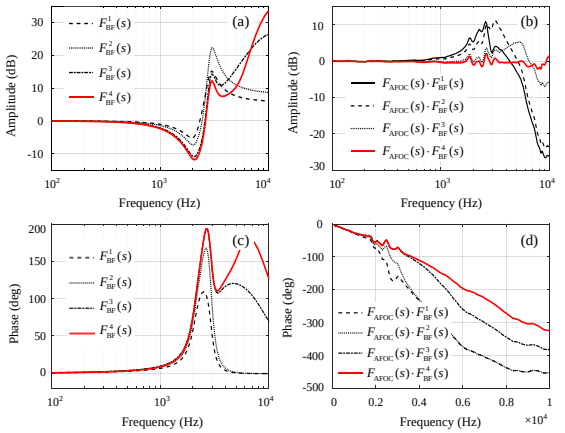

Figure 5: Amplitude-frequency characteristic of the biquad filters (a) and the compensated system (b); Phase-frequency characteristic of the biquad filters (c) and the compensated system (d).

compensated system gradually tends to a pure delay system with an inherent response delay of a fixed value.

A hardware processor is built and used to implement four cascaded digital biquad filters $F_{DBF}^4(s)$ that are expected to have the same frequency characteristics of $F_{BF}^4(s)$. The filters are inserted between the controller and HVA. The tested frequency characteristics of the filters $F_{DBF}^4(s)$ and the compensated system $F_{AFOC}(s)\cdot F_{DBF}^4(s)$ are shown in Figure 6. Figure 6(a) shows that when the frequency is within 10 kHz, the amplitude-frequency characteristic of the compensated system $F_{AFOC}(s)\cdot F_{DBF}^4(s)$ is almost completely flattened, and its fluctuations are suppressed in ±3 dB. In Figure 6(b), it can be seen that the phase-lagging of $F_{AFOC}(s)\cdot F_{DBF}^4(s)$ is compensated to -51° at 2 kHz, and the characteristic curve also almost overlap with the inherent response delay module $e^{-(8.8e\text{-}05)s}$. The results indicate that the compensated system $F_{AFOC}(s)\cdot F_{DBF}^4(s)$ has been successfully transformed into a pure delay system with inherent response delay of about 88 μs.

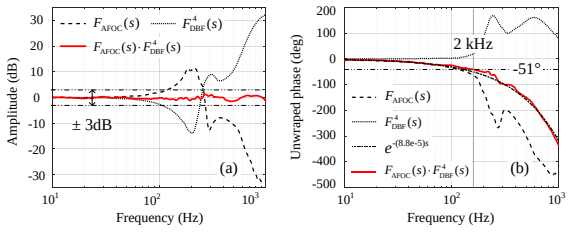

Figure 6: Amplitude-frequency characteristic (a) and phase-frequency characteristic (b) of the cascaded digital biquad filters and the compensated system.

4 COHERENT BEAM COMBINATION

Methods presented in part 2 and part 3 work according to the time-domain and frequency-domain characters of the AFOC respectively. Method of active resonance suppression deals with the voltage signals applied on the AFOC and is independent from the system framework where the AFOC is used. PD-SPGD algorithm needs the metric information, like the coupled power as shown in part 2. PD-SPGD could also be utilized in CBC system where the metric is related with each laser beam of the AFOCs array. Here we present the researches about CBC based on both PD-SPGD and active resonance suppression method.

A two-channel CBC experiment using active resonance suppression method and PD-SPGD algorithm is conducted. The structural scheme is shown in Figure 7. In this structure, the tip/tilts control voltages are only applied to the *X*-direction of AFOC-1 (the direction which we measured and filtered before), and the filters $F_{DBF}^4(s)$ are inserted between the controller and HVA. In addition, the laser beam emitted by AFOC-2 is well overlapped with the pinhole placed in front of the photo-detector.

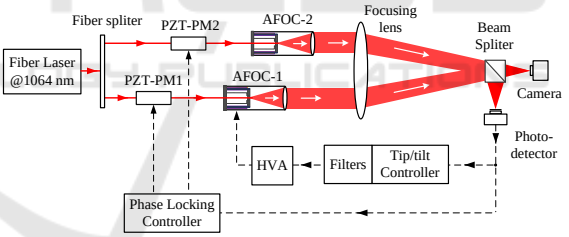

Figure 7: Structural scheme of the two-channel CBC experiment.

Firstly, common SPGD algorithm with iteration rate of 20 kHz and 1.6 kHz is employed as the control strategy for phase locking and tip/tilts control separately. The iteration curve of the normalized performance metrics *J* and the long-exposure far-field intensity distributions acquired by the camera are shown in Figure 8. The operation status contains four different steps: (I) two control loops didn't perform any correction; (II) only the phase locking control was performed; (III) both phase locking and tip/tilts control were performed, whereas the filters were not used; (IV) filters were used on the basis of the precious step. By means of only correcting piston errors with PZT-PMs in step (II), the average of *J* was increased by 73%. When

the static tip/tilt errors were corrected in step (III), the average of *J* was increased by 39%. When the filters were used in step (IV), the average of *J* did not show a significantly change, and there was no clearly difference in the corresponding long-exposure far-field intensity distributions. However, the corresponding MSE and the dithering range of *J* were decreased by 37% and 38% in step (IV). This result indicates that the stability of the closed-loop performance metrics *J* has improved by the biquad filters.

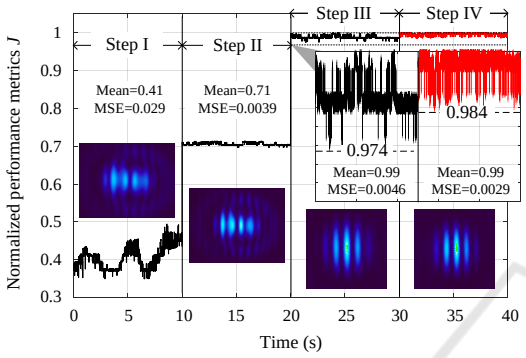

Figure 8: Structural scheme of the two-channel CBC experiment.

In a follow-up experiment, the phase locking control and the active resonance suppression method are performed together, and the PD-SPGD algorithm is used to compensate for the inherent response delay of about 88 μs in the tip/tilts control loop. The iteration rate of PD-SPGD algorithm set up here is 6 kHz and the sampling rate is 60 kHz. As shown in Figure 9, the traditional SPGD algorithm (with the filters) diverges at the iteration rate of 6 kHz, whereas the PD-SPGD algorithm (with the filters) converged. This result indicates that the inherent response delay becomes the main reason for the limited iteration rate of SPGD when the resonance is suppressed, and the iteration rate is successively increased to 6 kHz when the inherent response delay is compensated by the PD-SPGD.

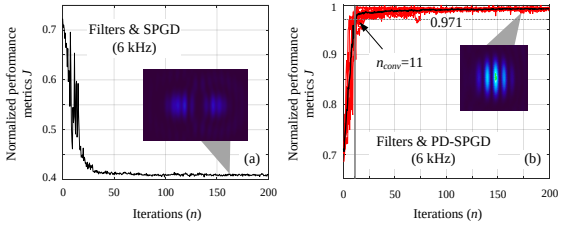

Figure 9: Iteration curve of normalized performance metrics J of SPGD and PD-SPGD with iteration rate of 6 kHz.

As a typical blind optimization algorithm, the higher control bandwidth of SPGD depends on the shorter convergence time, which is determined not only by the iteration rate, but also by the iterations required to converge. Experimental results show that the PD-SPGD algorithm (with appropriate parameter setting) can improve the iteration rate without interfering too much with the convergence iteration number of the convergence steps. This conclusion is reconfirmed in Figure 10, which shows the averaged iteration cure of the SPGD algorithm and the PD-SPGD algorithm with iteration rate of 1.6 kHz and 6 kHz. Each curve is obtained by averaging ten sets of data, and the convergence iteration number of the convergence steps can be counted as 9 and 11. Therefore, the actual convergence time is 5.63 ms and 1.83 ms for SPGD and PD-SPGD algorithm respectively. Results from this experiment indicate that the actual control bandwidth of AFOC will be 3.1 times higher than before by the biquad filters and the PD-SPGD algorithm.

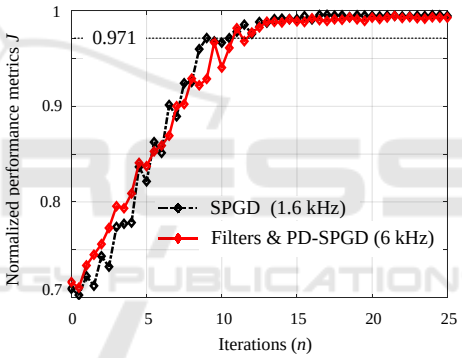

Figure 10: Averaged iteration curve of the SPGD and the PD-SPGD with iteration rate of 1.6 kHz and 6 kHz.

5 CONCLUSIONS

In this paper, we have reported on the research progress of the tip/tilts control bandwidth promotion for beam combining application in IOE, CAS. Two methods, inherent response delay compensation and active resonance suppression, are proposed and experimentally validated. The resonance suppression experiment tells that the amplitude-frequency characteristic of AFOC has been completely flattened by the biquad filters, and its fluctuations are suppressed in ±3 dB when the frequency is within 10 kHz. AFOC's phase-frequency characteristic is also compensated approximatively to a pure delay element. CBC experiment results show that the actual control bandwidth has been 3.1

times higher than before when the filters and the PD-SPGD algorithm are performed simultaneously. Obviously, the AFOCs with higher control bandwidth give the CBC system abilities to cope with stronger atmospheric turbulence. These results give great prospects to future applications that utilize fiber-array BD as the optical transceiver.

This work is supported in part by the National Natural Science Foundation of China under grant No. 61675205 and in part by the CAS "Light of West China" program.

REFERENCES

Filimonov, G. A., Vorontsov, M. A., Lachinova, S. L., 2014. Performance analysis of a coherent tiled fiber-array beam director with near-field phase locking and programmable control of tip/tilt and piston phases. Proc. SPIE 8971/9, 1-6.

Vorontsov, M., Weyrauch, T., Beresnev L., Carhart G., Liu, L., Aschenbach K., 2009. Adaptive array of phase-locked fiber collimators: analysis and experimental demonstration. IEEE J. Sel. Top. Quantum Electron. 15/2, 269–280.

Yu, C. X., Augst, S. J., Redmond, S. M., 2011. Coherent combining of a 4kW, eight-element fiber amplifier array. Opt. Lett. 36/14, 2686-2688.

Vorontsov, M. A., Filimonov, G., Ovchinnikov, V., Polnau, E., Lachinova, S. L., Weyrauch, T., Mangano, J., 2016. Comparative efficiency analysis of fiber-array and conventional beam director systems in volume turbulence. Appl. Opt. 55/15, 4170–4185.

Weyrauch, T., Vorontsov, M. A., Mangano, J., Ovchinnikov, V., Bricker, D., Polnau, E. E., Rostov, A. P., 2016. Deep turbulence effects mitigation with coherent combining of 21 laser beams over 7 km. Opt. Lett. 41/4, 840-843.

Geng, C., Luo, W., Tan, Y., Liu, H., Mu, J., Li, X., 2013. Experimental demonstration of using divergence cost-function in SPGD algorithm for coherent beam combining with tip-tilt control. Opt. Express 21/21, 25045–25055.

Geng, C., Zhao, B., Zhang, E., Luo, W., Tan, Y., Zhu, Y., Yang, H., Mu, J., Li, X., Duan, K., Zhao, W., 2013. 1.5 kW Incoherent beam combining of four fiber lasers using adaptive fiber-Optics collimators. IEEE Photon. Technol. Lett. 25/13, 1286-1289.

Li, F., Geng, C., Huang, G., Yang, Y., Li, X., Qui, Q., 2017. Experimental demonstration of coherent combining with tip/tilt control based on adaptive space-to-fiber laser beam coupling. IEEE Photon. J. 9/2, 7102812.

Luo, W., Geng, C., Wu, Y., Tan, Y., Luo, Q., Liu, H., Li, X., 2014. Experimental demonstration of single-mode fiber coupling using adaptive fiber coupler. Chin. Phys. B 23/1, 014207.

Yang, Y., Geng, C., Li, F., Huang, G., Li, X., 2017. Coherent polarization beam combining approach based on polarization controlling in fiber devices. IEEE Photon. Technol. Lett. 29/12, 945-948.

Yang, Y., Geng, C., Li, F., Huang, G., Li, X., 2017. Multi-aperture all-fiber active coherent beam combining for free-space optical communication receivers. Opt. Express 25/22, 27519–27532.

Li, F., Geng, C., Li, X., Qui, Q., 2015. Co-aperture transceiving of two combined beams based on adaptive fiber coupling control. IEEE Photon. Technol. Lett. 27/17, 1787–1790.

Liu, L., Vorontsov, M. A., Polnau, E., Weyrauch, T., Beresnev, L. A., 2007. Adaptive phase-locked fiber array with wavefront phase tip-tilt compensation using piezoelectric fiber positioners. Proc. SPIE 6708/0K, 1-12.

Geng, C., Li, X., Zhang, X., Rao, C., 2011. Coherent beam combination of an optical array using adaptive fiber optics collimators. Opt. Commun. 284/24, 5531–5536.

Beresnev, L., Vorontsov, M., 2005. Design of adaptive fiber optics collimator for free-space communication laser transceiver. Proc. SPIE. 5895, 58950R-1–58950R-7.

Huang, G., Geng, C., Li, F., Yang, Y., Li, X., 2018. Adaptive SMF coupling based on precise-delayed SPGD algorithm and its application in free space optical communication. IEEE Photon. J. 10/3, 7904212.